Effect of Pressure on Islet Amyloid Polypeptide Aggregation: Revealing the Polymorphic Nature of the Fibrillation Process[†]

Diana Radovan, Vytautas Smirnovas, and Roland Winter*

Department of Chemistry, Physical Chemistry I-Biophysical Chemistry, Dortmund University of Technology, D-44227 Dortmund, Germany

Received March 24, 2008; Revised Manuscript Received April 29, 2008

ABSTRACT: Type II diabetes mellitus is a disease which is characterized by peripheral insulin resistance coupled with a progressive loss of insulin secretion that is associated with a decrease in pancreatic islet β-cell mass and the deposition of amyloid in the extracellular matrix of β-cells, which lead to islet cell death. The principal component of the islet amyloid is a pancreatic hormone called islet amyloid polypeptide (IAPP). High-pressure coupled with FT-IR spectroscopic and AFM studies were carried out to elucidate further information about the aggregation pathway as well as the aggregate structures of IAPP. To this end, a comparative fibrillation study of IAPP fragments was carried out as well. As high hydrostatic pressure (HHP) is acting to weaken or even prevent hydrophobic self-organization and electrostatic interactions, application of HHP has been used as a measure to reveal the importance of these interactions in the fibrillation process of IAPP and its fragments. IAPP preformed fibrils exhibit a strong polymorphism with heterogeneous structures, a large population of which are rather sensitive to high hydrostatic pressure, thus indicating a high percentage of ionic and hydrophobic interactions and loose packing of these species. Conversely, fragments 1−19 and 1−29 are resistant to pressure treatment, suggesting more densely packed aggregate structures with less void volume and strong cooperative hydrogen bonding. Furthermore, the FT-IR data indicate that fragment 1−29 has intermolecular β-sheet conformational properties different from those of fragment 1−19, the latter exhibiting polymorphic behavior with more disordered structures and less strongly hydrogen bonded fibrillar assemblies. The data also suggest that hydrophobic interactions and/or less efficient packing of amino acids 30−37 region leads to the marked pressure sensitivity observed for full-length IAPP.

Proteins are able to form different types of insoluble aggregates. On one hand, amorphous aggregates may be formed, which have multiple protein conformations with rather ill-defined intermolecular interactions. On the other hand, more ordered protein structures such as amyloid fibrils may be formed. Upon formation of amyloid fibrils, the protein molecules that compose the fibrils (partially) lose their native conformation and generally adopt ordered, stacked cross-β-sheet structures (*1*–*4*). Protein amyloid formation and accumulation are implicated in a number of diseases, such Alzheimer's and Parkinson's disease, type II diabetes mellitus (TIIDM),[1] and prion disorders (*1*–*4*), and seem to be important factors in the development of the symptoms of these diseases. An interesting feature of fibril structures is their polymorphism (*5*–*7*).

Despite the recent advances in the theoretical and experimental techniques used to understand these aggregation processes, the underlying mechanisms have proven to be challenging to study. This is essentially due to the very low solubility of amyloidogenic peptides and the irreversibility of protein aggregation under ambient temperature and pressure conditions, which complicates or even prohibits the analysis of the underlying kinetic, thermodynamic, and structural parameters. Also, the origin of fibril polymorphism is still largely unknown. It may be caused by a polymorphism of the protofilaments forming the mature fibrils, or the polymorphism may represent different ways of organizing otherwise identical protofilaments. Understanding the polymorphic nature of protein fibrils may be important in understanding the ability of diseases to transmit between individuals, sometimes crossing the species barrier as in the case of prion protein.

In this work, we study the highly amyloidogenic islet amyloid polypeptide (IAPP). IAPP is a 37-amino acid peptide hormone (*8*) that is cosynthesized and cosecreted with insulin by pancreatic β-cells (*9*). Several functions have been associated with the soluble form of this hormone (*9*–*13*), including the control of hyperglycemia by restraining the rate at which dietary glucose enters the bloodstream. IAPP aggregates in the extracellular matrix of the β-cells forming fibrillar amyloid deposits. These deposits are present in

[†] Financial support from the Deutsche Forschungsgemeinschaft (DFG), the Fonds der Chemischen Industrie, and NRW/EU (Europäischer Fonds für regionale Entwicklung) is gratefully acknowledged.

* To whom correspondence should be addressed. Phone: +49 231 755 3900. Fax: +49 231 755 3901. E-mail: roland.winter@tu-dortmund.de.

[1] Abbreviations: IAPP, islet amyloid polypeptide; hIAPP, human IAPP; FT-IR, Fourier-transform infrared; AFM, atomic force microscopy; HHP, high hydrostatic pressure; TIIDM, type II diabetes mellitus; TFE, 2,2,2-trifluoroethanol; HFIP, hexafluoro-2-propanol; ThT, thioflavin T; β2-m, β_2-microglobulin; TTR, transthyretin.

10.1021/bi800503j CCC: $40.75
Published on Web 05/23/2008

approximately 95% of TIIDM patients and are strongly associated with islet β-cell degeneration and loss (*14, 15*). It has been demonstrated that the initial stages of IAPP fibril formation are driven by the increase in the level of solvent exposure of hydrophobicity patches (*16*) and that the IAPP aggregation process has two distinct phases, a lateral growth of oligomers and a longitudinal growth into mature fibrils (*16–18*). The structural changes behind the fibrillation process are still poorly understood, however.

Since the three-dimensional structure of IAPP is not yet known, experimental studies on fragments of this peptide can provide further insights into the mechanism of aggregation. Several studies indicate that amino acid residues 20−29 make up the main amyloidogenic region (*19, 20*), with a particular emphasis on the penta- and hexapeptide sequences IAPP 23−27 (FGAIL) and IAPP 22−27 (NFGAIL), respectively, as minimal peptide sequences required for aggregation (*21*). On the other hand, fragments IAPP 15−19 (FLHVS) and IAPP 14−18 (NFVHL) and the possible importance of aromatic residues (and thus $\pi-\pi$ interactions) for amyloid fibril formation were also discussed (*21, 23*), while the N-terminal region of residues 1−19 may be essential for the interaction with membranes (*24, 25*). Region 1−13, however, has been reported not to form fibrils (*26*). On the other hand, it has been reported that IAPP 8−20 is able to form fibrils (*26*). To complement these studies, we decided to inspect also the aggregation of synthetic human IAPP 1−19 N-amidated and human IAPP 1−29 C-terminally amidated, both containing a disulfide bridge between Cys 2 and Cys 7, in comparison with the full-length peptide. The amidation was carried out for a more realistic comparison with the natural human hormone, in which this modification seems to play an essential role in its hormonal function in vivo (*27*).

High hydrostatic pressure (HHP) has been widely used as a tool in understanding protein stability and folding (*28–39*). High pressure tends to destabilize proteins due the fact that the protein−solvent system in the unfolded state occupies a smaller volume than the system in the native state. In a similar way, pressure leads to the dissociation of oligomeric proteins. These effects seem to be caused by a combination of factors. The presence of cavities within the folded proteins or in the interface of oligomers favors unfolding or dissociation of these structures. The dissociation of electrostatic interactions also leads to a marked reduction in the overall volume caused by electrostrictive effects of the water molecules around the unpaired polar and charged residues. These effects compensate for the increase in volume as the protein interior is disrupted, exposed to solvent, and hydrated upon unfolding. Finally, hydrophobic interactions have been shown to weaken upon pressurization (*40*).

Temperature-induced aggregation generally results in an irreversible aggregation process, which may be explained by less disfavored hydrophobic interactions at higher temperatures. On the contrary, denaturation by high pressure generally is a reversible process. Furthermore, high-pressure treatment can lead to dissociation of aggregated structures and may result in formation of monomers and natively folded structures (*33, 35, 41–43*). Hence, in addition to cosolvent and temperature perturbation, pressure-dependent studies are able to shed new light on alternative folding−aggregation pathways and their intermediate states.

Because of the fact that high hydrostatic pressure acts to disfavor hydrophobic and electrostatic interactions that cause protein aggregation, pressure-axis experiments are used in this study as an efficient tool to elucidate new information about the fibrillation processes and the polymorphic states of IAPP and fragments thereof. High pressure coupled with Fourier-transform infrared (FT-IR) spectroscopic studies and atomic force microscopy (AFM) measurements are used to reveal the changes in the peptide's aggregate and fibril formation under pressure perturbation. These results lead to a more complete understanding of the aggregation pathways and the possible amyloidogenic states of IAPP and its fragments and may hence contribute to a better understanding of the pathogenesis of type II diabetes mellitus.

MATERIALS AND METHODS

Synthetic human IAPP (hIAPP) was obtained from Calbiochem-Novabiochem (Bad Soden, Germany). Synthetic human IAPP 1−19 N-amidated and human IAPP 1−29 C-terminally amidated, both containing a disulfide bridge between Cys 2 and Cys 7, were obtained from PSL (Peptide Specialty Laboratory, Heidelberg, Germany). NaH_2PO_4 buffer was purchased from Gibco BRL, and 2,2,2-trifluoroethanol (TFE) was obtained from Aldrich. HFIP (hexafluoro-2-propanol), ThT (thioflavin T), D_2O, and all other reagents were from Sigma. The reagents were of the highest analytical grade available. Predistilled water was filtered and deionized through a Millipore purification system.

Incubation under pressure was carried out in a pressure cell equipped with sapphire optical windows, similar to that originally described by Paladini and Weber (*44, 42*). The temperature of the pressure cell was controlled by means of a jacket connected to a circulating bath. Pressure was increased stepwise in increments of 150 bar until 3.5 kbar.

IAPP stock solutions were kept in 100% TFE at −20 °C and diluted prior to the experiments to give the chosen final concentration [in 50 mM NaH_2PO_4 (pH 7.4)], with residual 1% TFE. In an alternative fashion, IAPP and the fragments used in this study (1−19 and 1−29) were dissolved in 100% HFIP and corresponding amounts from the stock solutions were subjected to overnight lyophilization under vacuum prior to rehydration in buffer.

For the FT-IR measurements, CaF_2 transmission windows with 0.05 mm Teflon spacers were used. The temperature in the cell was controlled with an external water circuit. FT-IR spectroscopy has proven to be a powerful technique for determining the secondary structure elements (*33, 39, 45, 46*). The amide I′ band (between 1600 and 1700 cm^{-1}) was recorded, which is mainly associated with the carbonyl stretching vibration of the amide groups and which is directly related to the backbone conformation and hydrogen bonding pattern of the protein. For scanning the samples before and after pressure treatment, we used 50 mM NaH_2PO_4 (with 1% residual TFE in D_2O for IAPP) at pD 7.4 and a protein concentration of 0.1% (w/w) and additionally 0.5% (w/w) for the fragments. The FT-IR spectra were recorded on a Nicolet 5700 FT-IR spectrometer equipped with a liquid nitrogen-cooled MCT detector. For the fragment studies, spectra were recorded every 5 min for 20 h. For each spectrum, 256 interferograms of 2 cm^{-1} resolution were coadded. The sample chamber was continuously purged with

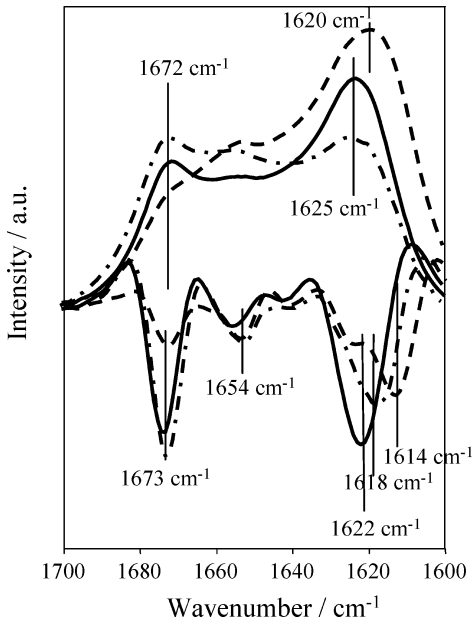

FIGURE 1: FT-IR spectra (at the top) of IAPP (—) freshly dissolved sample at time zero, (—•—) after aggregation for 3 days in 50 mM NaH_2PO_4 (pD 7.4) at ambient pressure, and (– – –) after 3 days at 3.5 kbar. All data were taken at 25 °C. At the bottom of the figure, the second-derivative spectra are shown, which allow a more accurate determination of peak positions.

dry air. From the spectrum of each sample, a corresponding buffer spectrum was subtracted. All the spectra were baseline-corrected and normalized for the amide I′ band area. Data processing was performed with GRAMS.

For the atomic force microscopy (AFM) measurements, samples were diluted with deionized water to yield a final concentration of 1 μM. From this diluted solution, 20 μL was applied onto freshly cleaved muscovite mica and allowed to dry. Data were acquired in the tapping mode on a Multi Mode TM SPM AFM microscope equipped with a Nanoscope IIIa controller from Digital Instruments. As AFM probes, Silicon SPM Sensors "NCHR" (force constant, 42 N/m; length, 125 mm; resonance frequency, 300 kHz) from Nanosensors were used (*36, 46*).

RESULTS

High-Pressure Studies on Full-Length IAPP. To investigate the stability of IAPP toward high pressure, either fresh peptide or preformed IAPP fibrils were subjected to pressures up to 3.5 kbar (350 MPa), and the changes were monitored by FT-IR spectroscopy and AFM to yield information about the transformation process and the structures evolving at various levels of complexity. The protein solutions were prepared from stock solutions in a water buffer with 1% residual TFE. Such a condition has been shown to give rise to or to synchronize the formation of preassembled β-sheet structures which are rich in fibrils and protofibrils (*47*). FT-IR spectroscopy was used to monitor the secondary conformational changes, a common tool used to monitor conformational transitions and to disentangle different β-sheet structures that accompany protein aggregation processes that can also be used to carry out pressure-dependent studies (*33, 39, 45*). Figure 1 shows FT-IR spectra of various IAPP samples: freshly dissolved IAPP and IAPP aggregated for 3 days at ambient pressure and at 3.5 kbar, respectively. All spectra were recorded at room temperature (25 °C). The FT-IR spectrum of the freshly prepared IAPP sample (5 min after preparation) at a concentration as high as 0.1% (w/w) exhibits an intense IR band appearing at ~1622 cm^{-1}, which is due to intermolecular parallel β-sheet structures, and a pronounced peak at 1673 cm^{-1}, which is due to turns and residual trifluoroacetic acid (TFA) in the sample. Such an IR pattern is indicative of the aggregated state of IAPP according to data of other amyloidogenic proteins, like insulin (*43, 46*). After the incubation period of 3 days at ambient temperature and pressure, the IR spectrum exhibits similar features, with a broadening and a small shift of the amide I′ band to slightly smaller wavenumbers (~1618 cm^{-1}), however. Very likely, a distribution of different sizes and shapes of IAPP aggregate is found initially, and the overall size of the structures evolving increases with an increase in IAPP concentration. After the incubation period, it seems that the β-strands are realigning from a nonperfectly packed initial state to more ordered structures with stronger H-bonding, leading to the observed shift of the amide I′ band to 1618 cm^{-1} accompanied by an increase in the β-turn content. When IAPP was aggregated under pressure (3.5 kbar), the aggregate band shifts to significantly smaller wavenumbers (~1614 cm^{-1}), indicating that the pressure treatment leads to the formation of a different aggregate structure with stronger intermolecular H-bonding between β-sheet strands, or to a larger population of these species.

To reveal the different morphological structures formed, AFM measurements were carried out for this IAPP concentration under the same preparation conditions (Figure 2). Most of the aggregate structures seen in the sample that was not subjected to HHP are short (<1 μm) fibrils with average diameters of 5−15 nm as determined from the AFM height profile. Such rather short fibrillar structures probably appear due to a comparably fast nucleation process at this rather high peptide concentration. The pressure-treated sample (Figure 2B) still contains fibrils, but also a significant amount of smaller oligomeric particles (0.5−1.5 nm in size).

Taking the FT-IR spectroscopic and AFM results together, we may conclude that the sample subjected to high-pressure treatment displays less fibrillar β-sheet structures and a larger population of smaller amorphous aggregates with a different H-bonding pattern. To support these conclusions, the samples with and without 3 days of pressure treatment were centrifuged at 16000 rpm and 4 °C for 20 min to remove any insoluble material and the protein concentration of the supernatant was determined from the UV absorbance at 274.5 nm, using a molar extinction coefficient of 1440 M^{-1} cm^{-1} (*16*). Protein was detected only for the pressurized IAPP (~17% of the overall protein concentration). Immediately after the absorbance measurements, also far-UV CD spectra were recorded. The HHP-treated sample exhibited a strong negative band at 200 nm and a positive band at 230 nm, characteristic of the presence of unordered structures (data not shown). The different fibrillar and nonfibrillar amorphous/oligomeric morphologies found for the high-pressure-treated sample indicate that not all IAPP aggregate structures are equally sensitive to pressure, hence suggesting the existence of pressure resistant fibrils with densely packed cores and a population that can be dissociated by HHP.

Kinetics of Aggregation of IAPP and IAPP Fragments. We also carried out a detailed comparative kinetic study of

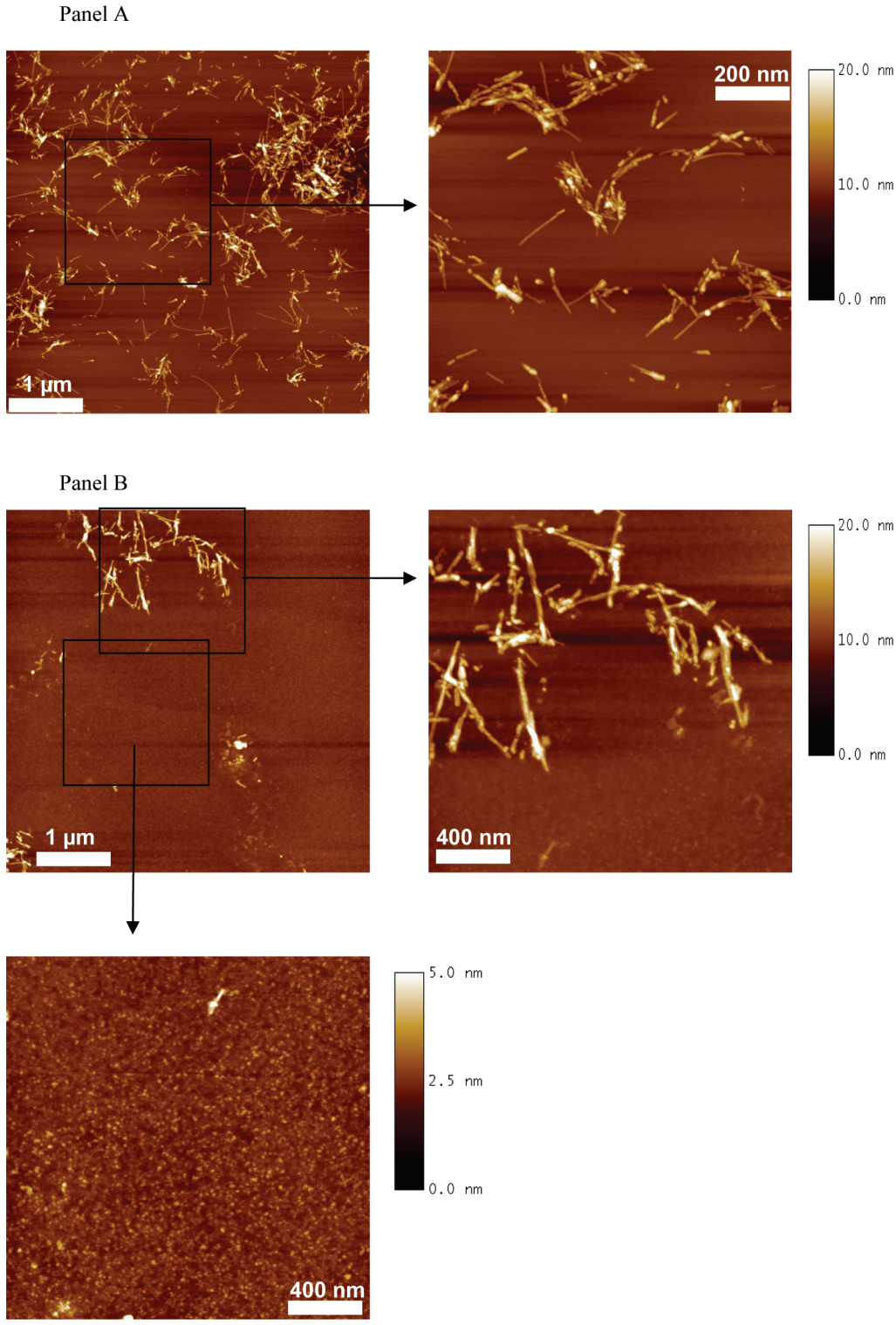

FIGURE 2: AFM height images of 0.1 wt % IAPP aggregates after 3 days without (A) and with pressure treatment at 3.5 kbar (B). The same samples analyzed by FT-IR spectroscopy were diluted with deionized water to yield a final concentration of 1 μM. Twenty microliters was applied onto freshly cleaved muscovite mica and allowed to dry before the AFM analysis (*39*).

the aggregation−fibrillation reaction of hIAPP, hIAPP 1−19, and hIAPP 1−29 in neutral buffer at 37 °C by FT-IR spectroscopic analysis. The peptides were originally dissolved in HFIP (hexafluoro-2-propanol) and subjected to overnight lyophilization prior to rehydration in buffer. Whereas the full-length IAPP readily forms fibrils even at concentrations in the low micromolar range, the aggregation reaction of the fragments occurs in a reasonable time range at much higher concentrations, only. Hence, kinetic experiments were carried out with 0.1 and 0.5% (w/w) solutions at 37 °C. All freshly dissolved peptides analyzed by FT-IR spectroscopy show a predominantly disordered conformation at time zero (Figure 3A), indicated by a broad amide I′ peak at ~1642−1644 cm^{-1}. Both full-length IAPP and IAPP 1−29 already contain a significant amount of β-sheet structures from the very beginning of the experiment at these concentrations. A characteristic shift from random coil to β-sheet structures is observed for all three peptides, with a significant amount of

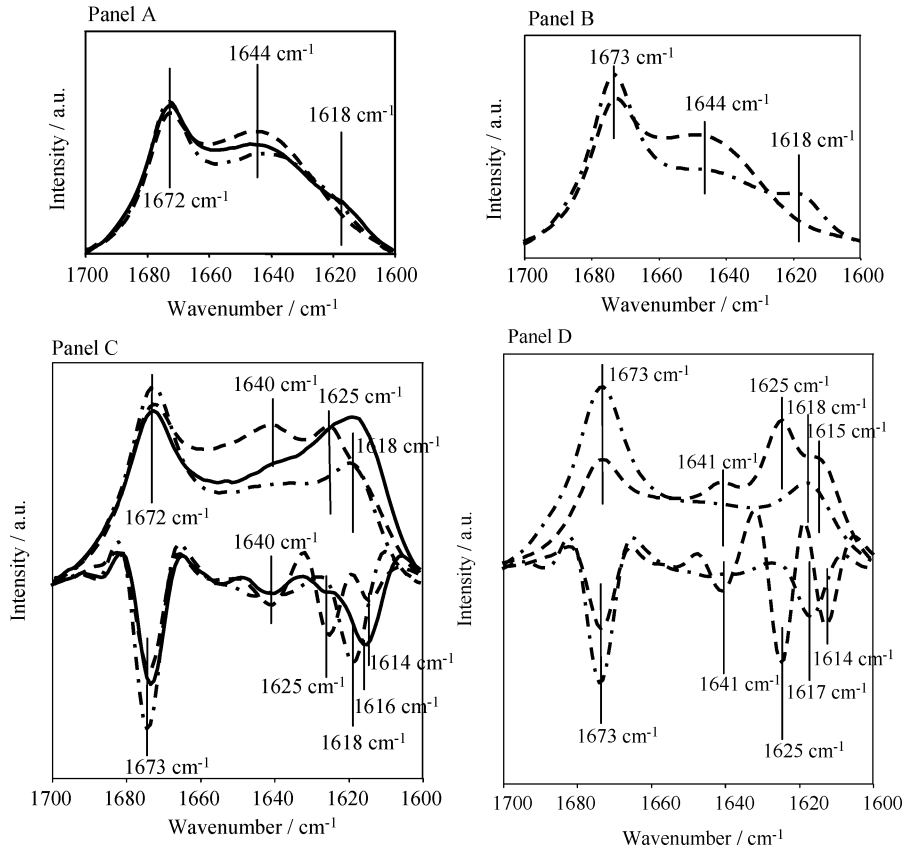

FIGURE 3: FT-IR spectra of freshly dissolved IAPP and fragments of IAPP at a concentration of 0.1 (A) and 0.5 wt % (B): (—) IAPP, (– – –) IAPP 1−19, and (–•–) IAPP 1−29. In panels C (0.1 wt %) and D (0.5 wt %), the IR spectra collected at the end of the experiment (after 24 h) and the corresponding second-derivative spectra are shown, which allow a more accurate determination of peak positions. All data were recorded at 37 °C in 50 mM phosphate buffer (pD 7.4).

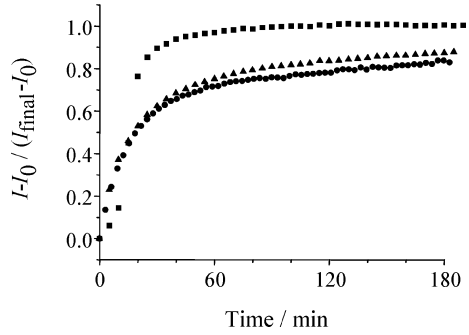

FIGURE 4: Kinetics of the aggregation process for all three [(■) IAPP, (▲) IAPP 1−19, and (●) IAPP 1−29] based on the normalized maximum peak intensities in the β-sheet region of the amide I′ band. All data were recorded at 37 °C in 50 mM phosphate buffer (pD 7.4).

random/turn structures still present in the case of the two fragments even after 24 h (Figure 3C). As revealed in Figure 3C, the random coil to β-sheet conversion is much more pronounced for the full-length IAPP in comparison to the fragments. The position of the IR aggregate bands occurs at slightly different positions: at 1625 cm^{-1} for IAPP 1−19, at ~1618 cm^{-1} for IAPP 1−29, and at 1616−1618 cm^{-1} for full-length IAPP. For both IAPP fragments 1−19 and 1−29, the shift from random coil to β-sheet conformation occurs rather rapidly within the first 20 min, followed by a much slower increase in β-sheet content, not reaching plateau values even after 3 h (Figure 4). Conversely, for full-length IAPP, after a slightly slower initial nucleation process, the random to β-sheet conversion is completed after 40 min. To ensure sufficient time for complete fibril maturation in all three cases, we incubated samples prepared in the same manner as for the FT-IR experiments at 37 °C for 24 h prior to taking aliquots for the AFM analysis (Figure 5). Due to the peak of the remaining TFA in the sample, peak fitting of the data is not very precise, the β-sheet content of the mature fibrillar state can be estimated only from the FT-IR data, also assuming similar transition dipole moments for the various conformers. The β-sheet content at the end of the experiment (after ~20 h) is higher than 50% for IAPP, ~32% for IAPP 1−19, and ~27% for IAPP 1−29.

Via a comparison of the second-derivative IR spectra of the final fibrillar structures (Figure 3C), it can be seen that fragment 1−29 is the only one with a single peak in the β-sheet region, which appears at 1618 cm^{-1}. IAPP 1−19 shows two β-peaks, a major one at 1625 cm^{-1} and a small one at ~1611−1614 cm^{-1}. For comparison, full-length IAPP shows a main peak at ~1616 cm^{-1} with a shoulder around 1625 cm^{-1}. Both full-length IAPP and fragment 1−19 exhibit an additional peak around 1640 cm^{-1} (much more pronounced for IAPP 1−29), indicating a significant population of remnant unordered structures.

The different wavenumbers assigned to individual peptide β-aggregate structures indicate different packing properties. The smaller the wavenumber, the stronger the H-bond strength of the intermolecular β-sheet structure. Hence, compared to IAPP and fragment 1−29, fragment 1−19 seems to form less strongly H-bonded and more disordered β-sheet fibrillar structures. Considering the fact that fragment 1−29 shows essentially one peak in the β-sheet region, only

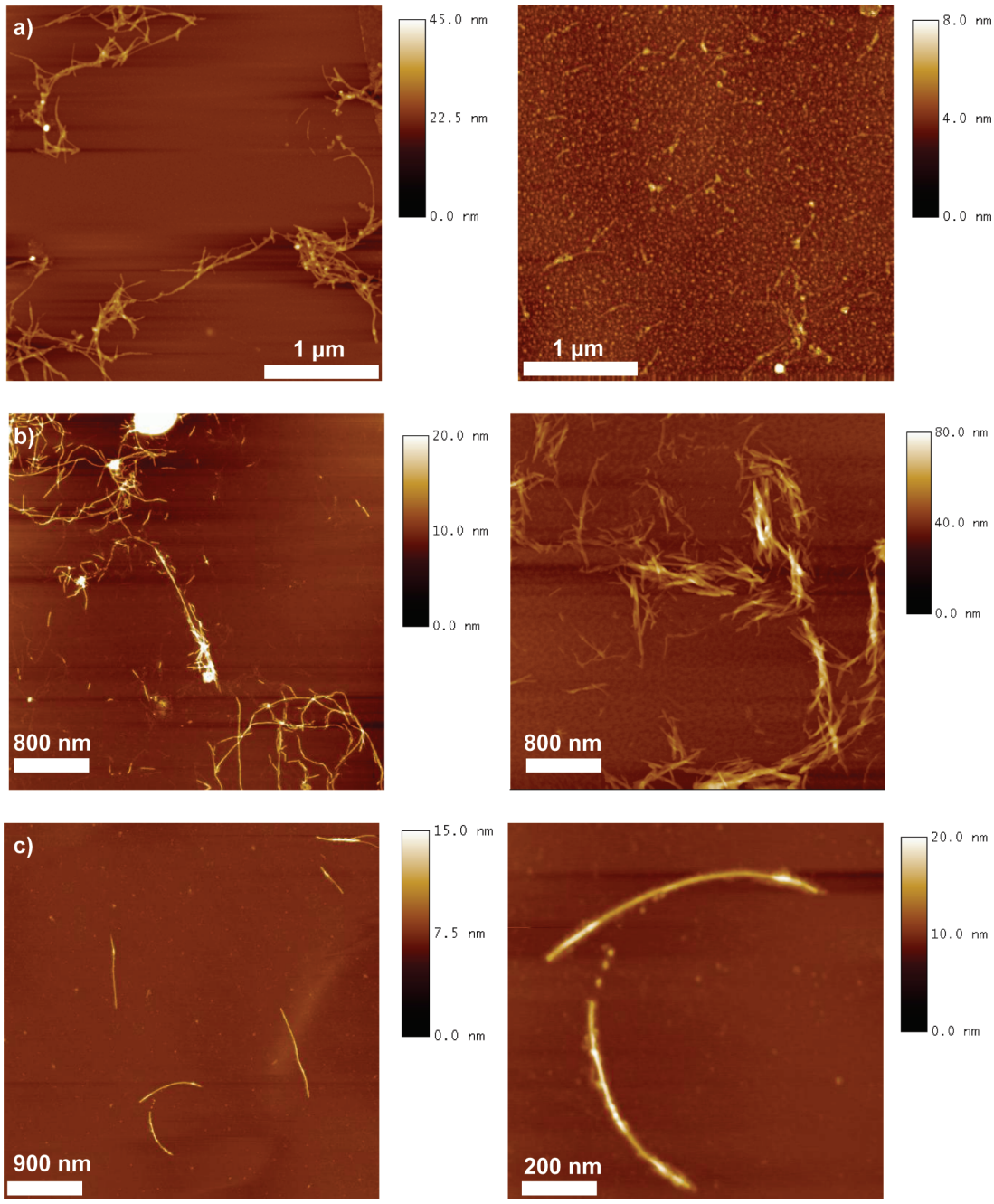

FIGURE 5: Selection of AFM height images of 0.1 wt % (a) IAPP 1−19, (b) IAPP 1−29, and (c) full-length IAPP aggregates after 24 h at 37 °C. Samples incubated under the same conditions as those measured in the FT-IR sample cell were diluted with deionized water to yield a final concentration of 1 μM. Twenty microliters was applied onto freshly cleaved muscovite mica and allowed to dry before the AFM analysis.

(at ~1618 cm^{-1}), this indicates that in fragment 1−29 the amino acid regions of residues 1−19 and 20−29 seem to take part in forming β-strands cooperatively and pack efficiently against each other.

To gain insight into the morphology and particular characteristics of the aggregate and/or fibril structures (size, length) formed by these three peptides, tapping-mode atomic force microscopy (AFM) studies were employed. Most aggregate structures seen for IAPP 1−19 (Figure 5a) under these preparation conditions are 1−2 μm long. The sample seems to be rather polymorphic, with a relatively large population of different aggregate types with probably correspondingly different hydrogen bonding patterns (see FT-IR data above). The following main types of structures can be identified: Fibrils 5−15 nm in height and 1−2 μm in length, similar to what is normally seen for full-length IAPP (Figure 2); thin protofibrils 1−2 μm in length and 0.5−1.5 nm in diameter; and thick and short fibrils <1 μm in length and 50 nm in thickness are observed, probably as a result of considerable lateral growth. In addition, some bent structures and a large population of oligomers (top right corner of Figure 5a) have been detected as well.

The corresponding fibrillar structures for IAPP 1−29 and full-length IAPP are shown in panels b and c of Figure 5, respectively. IAPP 1−29 also exhibits a polymorphic behavior forming different types of fibrillar structures upon aggregation, ranging in length from 200 nm up to 2 μm with diameters of 5−15 nm as seen for IAPP as well. The fibrils

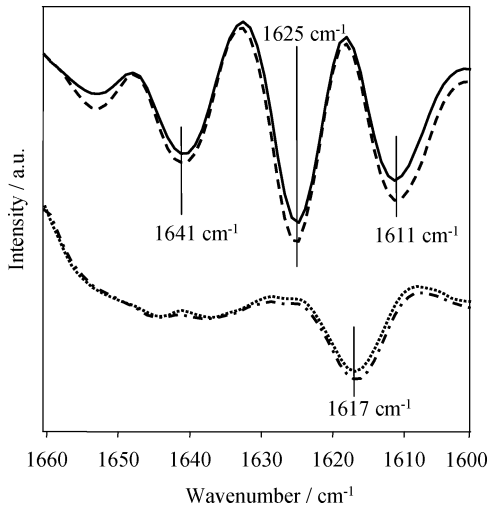

FIGURE 6: FT-IR spectra in the amide I′ band region and the corresponding second-derivative spectra of 0.5 wt % IAPP 1−19 (at the top of the figure) after aggregation for 24 h in 50 mM NaH_2PO_4 (pD 7.4) at ambient pressure (− − −) and after an additional 24 h at 3 kbar (—). At the bottom of the figure, the FT-IR spectra and the corresponding second-derivative spectra of IAPP 1−29 after aggregation for 24 h in 50 mM NaH_2PO_4 (pD 7.4) at ambient pressure (−•−) and after an additional 24 h at 3 kbar (•••) are shown. All data were recorded at 37 °C.

are often found to be branched, and sometimes bent fibrils are seen. Under these experimental conditions, IAPP forms mostly one type of fibril, 1−2 μm long with a diameter of 15 nm (Figure 5c). Often, bent structures are found as well. Oligomeric species and protofibrils are also present, but to a much smaller extent than for the IAPP fragments.

We have further increased the concentration of the fragments up to 0.5% (w/w). A similar kinetics of aggregation was observed as in the case of the 0.1% (w/w) solution. The spectral characteristics are also similar to those of the lower concentration (Figure 3B,D). For the IAPP 1−19 aggregate, we observe again two peaks, a major peak at 1625 cm^{-1} and a second one at 1611−1614 cm^{-1}, the latter being more pronounced at this higher concentration (Figure 3D). Hence, all the characteristics observed for the concentration of 0.1% (w/w) are observed at this higher concentration as well, including the AFM morphologies of the fibrillar structures that formed.

High-Pressure Studies on IAPP Fragments. High-pressure studies were carried out on both IAPP fragments and to reveal if high-pressure treatment is able to disrupt the mature fibrillar structures formed by fragments 1−19 and 1−29. Samples were first incubated at 37 °C for 24 h, thus allowing complete fibrillation. From these samples, aliquots were taken for the FT-IR spectroscopic and AFM analysis. The samples were then subjected to high hydrostatic pressure (3 kbar) for an additional 24 h at 25 °C.

Representative FT-IR results are shown in Figure 6. Unlike what we have previously observed for the pressurized full-length IAPP samples, the fragments show no major spectral changes when the pressure-treated samples are compared with the untreated ones. This suggests that the fragments form aggregates which are rather pressure-insensitive, i.e., contain densely packed cores which are more pressure-stable than the full-length IAPP aggregates. This obviously holds true for all aggregate structures present which have been detected by AFM analysis, the oligomeric and the fibrillar ones. In accordance with the FT-IR spectroscopic data, the AFM pictures of the pressurized samples did not exhibit significant morphological changes as well (data not shown).

DISCUSSION AND CONCLUSIONS

Here we report on high-pressure work with IAPP, including IAPP fragments, aim to reveal new information about their aggregation pathways and the structural properties and polymorphic nature of their aggregate and/or fibril structures. The conceptual framework for using such pressure-axis experiments is as follows: The interior of proteins is largely composed of rather efficiently packed residues (with a void volume on the order of ∼0.5%), more likely hydrophobic than those at the surface. High hydrostatic pressure induces conformational fluctuations due to a decrease in the strength of hydrophobic and electrostatic interactions, finally leading to partial pressure-induced unfolding through transfer of water molecules into the protein interior, gradually filling cavities and leading to the dissociation of close hydrophobic contacts and subsequent swelling of the hydrophobic protein interior (*39, 40*).

We point out in the introductory section that IAPP has not only one but several amyloidogenic cores that are interacting to form an organized aggregate structure and that hydrophobic interactions may drive the initial stage of the aggregation process. According to the literature, aggregation of the C-terminal domain of IAPP [amino acid residues 20−29 and 30−37 (*26*)] is thought to be most likely driven by hydrophobic interactions (*48*). Previous theoretical studies regarding secondary structure predictions of human IAPP indicate that there is one potential α-helical region between amino acid residues 8 and 14 and three potential β-strand regions. A β-turn has been predicted at Asn31, which would result in two adjacent β-strands (32−37 and 24−29); a third β-strand is proposed to exist in region 18−23 (*48*). These predictions have been complemented by experimental studies, showing aggregation into ordered fibrillar structures of fragments 8−20 and 8−37 as well (*19, 48*). Additionally, in our study, the comparison of the fibrillation of the different peptides indicates that IAPP 1−19, IAPP 1−29, and full-length IAPP are all three capable of self-assembly under similar conditions in vitro, to different extents, however. Interestingly, we found that fragment IAPP 1−19 is also prone to self-assembly and fibrillation. These findings suggest that the only region of IAPP reported not to form fibrils so far is region 1−13, to be more precise, region 1−8, which is the region exhibiting amino acid residues not prone to forming β-sheets. Rather, this region has been suggested to be responsible for membrane insertion (*24, 25*) and has most likely a modulating influence on conformational conversions and fibril formation (*48*).

As HHP is acting to weaken or even prevent hydrophobic self-organization and electrostatic interactions, we may expect that application of HHP may be used as a measure to reveal the importance of these interactions in formation of aggregates and/or fibrils of IAPP and its fragments. With all data taken together, a hypothetical model for IAPP fibril formation may be suggested: IAPP undergoes fast nucleation (due to several amyloidogenic "cores"), largely driven by hydrophobic interactions. Hence, formation and packing of fibrils are not perfect, and mixed-registry β-sheet structures

might exist, in particular at these high protein concentrations that were used, which can partially be dissociated by pressure leading to smaller aggregate structures and oligomers. An HHP as low as ~3 kbar is sufficient to weaken and (at least partially) disrupt the hydrophobic cores, thus leading to formation of a heterogeneous population of fibrillar aggregates with IR amide I′ bands in the low-wavenumber region (which is typical of a more strongly H-bonding pattern of intermolecular β-sheets) and a large amount of nonfibrillar smaller aggregates and oligomers, as detected by AFM. Our data also indicate that at least some of the preformed IAPP fibrils are sensitive to high hydrostatic pressure, similar to loosely packed, amorphous aggregates and inclusion bodies (*44, 49, 50*). Considering the fact that high hydrostatic pressure is an effective means of disturbing ionic and hydrophobic interactions but not hydrogen bonds, we can conclude that these former two types of interactions are also important for the stability of full-length IAPP fibrillar aggregates, as also suggested in work using denaturing agents (*16*).

Unlike full-length IAPP, the fragments investigated here exhibit an enhanced stability toward high-hydrostatic pressure treatment with maintenance of their fibrillar structures even up to pressures of 3 kbar. This points toward more densely packed aggregate structures with less defect volume and strong cooperative hydrogen bonding in these fragments when compared to full-length IAPP. The FT-IR data clearly indicate that fragment 1−29 has intermolecular β-sheet conformational properties different from those of fragment 1−19, the latter exhibiting polymorphic behavior with more disordered structures and less strongly H-bonded fibrillar assemblies. Obviously, hydrophobic interactions and electrostatic interactions as well as packing defects play a minor role in the IAPP 1−29 assemblies. Also, this indirectly implies that in the C-terminal region, hydrophobic interactions and/or less efficient packing for amino acid residues 30−37 (present in full-length IAPP, sensitive to high pressure) becomes more important than in fragment 20−29 (present in IAPP 1−29), which leads to the marked pressure sensitivity observed for full-length IAPP. The different molecular configurations of the peptides are probably the basis for the various structures and morphologies observed here. The packing of the residues outside the backbone region may constitute the observed polymorphisms.

CONCLUDING REMARKS

We have seen that the conformational stability of the fibrils varies, probably reflecting the difference in side chain packing inside the amyloid fibrils. A polypeptide's amino acid sequences are optimized by evolution for folding into the native conformation, but it is unlikely that a tight packing of the side chains can also be achieved for all residues in the non-native fibrillar structures (*51*). This is in accord with findings that amyloid fibrils made of short peptides or fragments of amyloidogenic proteins, such as of IAPP in this study or of TTR (*52, 53*), can be more densely packed. Presumably, in the case of many full-length polypeptide chains such as full-length IAPP, α-synuclein, and TTR, a dense packing can be achieved only in the core region(s) of the fibrils, leaving some loosely packed side chains in other regions. An amyloid structure without optimal packing is likely to enable formation of various isoforms, suggesting the structural basis of multiple forms of amyloid fibrils in contrast to the unique native fold of functioning proteins.

A disease caused by fibrillation of a protein often shows variations in terms of phenotypes and incubation periods. Such phenomena are termed strains and are thought to be connected to the fact that fibrils, also depending on the environmental conditions, can have various structural isoforms known as morphologies. Clearly, similar to, for example, insulin (*41*) and glucagon (*54*), also IAPP seems to belong to this class of amyloidogenic proteins. In analogy to the multiple-kinetic-pathway folding tunnel described by the energy landscape for globular protein folding, it seems to be very likely that there are generally also multiple routes to the formation of mature amyloid. Using the pressure variable, we are able to reveal additional details of the polymorphic forms of amyloid and its precursors as well as the transformation processes between these polymorphic states.

REFERENCES

1. Kelly, J. W. (1998) The alternative conformations of amyloidogenic proteins and their multi-step assembly pathways. *Curr. Opin. Struct. Biol. 8*, 101–106.
2. Dobson, C. M. (2001) The structural basis of protein folding and its links with human disease. *Philos. Trans. R. Soc. London, Ser. B 356*, 133–145.
3. Lansbury, P. T., Jr. (1992) In pursuit of the molecular structure of amyloid plaque: New technology provides unexpected and critical information. *Biochemistry 31*, 6865–6870.
4. Serpell, L. C., Sunde, M., Benson, M. D., Tennent, G. A., Pepys, M. B., and Fraser, P. E. (2000) The protofilament substructure of amyloid fibrils. *J. Mol. Biol. 300*, 1033–1039.
5. Kodali, R., and Wetzel, R. (2007) Polymorphism in the intermediates and products of amyloid assembly. *Curr. Opin. Struct. Biol. 17*, 48–57.
6. Goldsbury, C. S., Goldie, K. N., Müller, S. A., Saafi, E. L., Gruijters, W. T. M., Misur, M. P., Engel, A., Aebi, U., and Kistler, J. (1997) Polymorphic fibrillar assembly of human amylin. *J. Struct. Biol. 119*, 17–27.
7. Paravastu, A. K., Petkova, A. T., and Tycko, R. (2006) Polymorphic fibril formation by residues 10−40 of the Alzheimer's β-amyloid peptide. *Biophys. J. 90*, 4618–4629.
8. Lorenzo, A., and Yankner, B. A. (1994) β-Amyloid neurotoxicity requires fibril formation and is inhibited by congo red. *Proc. Natl. Acad. Sci. U.S.A. 91*, 12243–12247.
9. Cooper, G. J. S., Willis, A. C., and Leighton, B. (1989) Amylin hormone. *Nature 340*, 272.
10. Ohsawa, H., Kanatsuka, A., Yamaguchi, T., Makino, H., and Yoshida, S. (1989) Islet amyloid polypeptide inhibits glucose-stimulated insulin secretion from isolated rat pancreatic islets. *Biochem. Biophys. Res. Commun. 160*, 961–967.
11. Fehmann, H. C., Weber, V., Goke, R., Goke, B., Eissele, R., and Arnold, R. (1990) Islet amyloid polypeptide (IAPP;amylin) influences the endocrine but not the exocrine rat pancreas. *Biochem. Biophys. Res. Commun. 167*, 1102–1108.
12. Silvestre, R. A., Peiro, E., Degano, P., Miralles, P., and Marco, J. (1990) Inhibitory effect of rat amylin on the insulin responses to glucose and arginine in the perfused rat pancreas. *Regul. Pept. 31*, 23–31.
13. Johnson, K. H., O'Brien, T. D., Betsholtz, C., and Westermark, P. (1992) Islet amyloid polypeptide: Mechanisms of amyloidogenesis in the pancreatic islets and potential roles in diabetes mellitus. *Lab. Invest. 66*, 522–535.
14. Westermark, P., and Wilander, E. (1978) The influence of amyloid deposits on the islet volume in maturity onset diabetes mellitus. *Diabetologia 15*, 417–421.
15. Hayden, M. R. (2002) Pancreatic islet amyloid in type 2 diabetes mellitus: A clinical and historical review. *Mol. Med. 99*, 495–498.
16. Kayed, R., Bernhagen, J., Greenfield, N., Sweimeh, K., Brunner, H., Voelter, W., and Kapurniotu, A. (1999) Conformational

transitions of islet amyloid polypeptide (IAPP) in amyloid formation in vitro. *J. Mol. Biol. 287*, 781–796.
17. Padrick, S. B., and Miranker, A. D. (2002) Islet amyloid: Phase partitioning and secondary nucleation are central to the mechanism of fibrillogenesis. *Biochemistry 41*, 4694–4703.
18. Green, J. D., Goldsbury, C., Kistler, J., Cooper, G. J. S., and Aebi, U. (2004) Human amylin oligomer growth and fibril elongation define two distinct phases in amyloid formation. *J. Biol. Chem. 279*, 12206–12212.
19. Goldsbury, C., Goldie, K., Pellaud, J., Seelig, J., Frey, P., Muller, S. A., Kistler, J., Cooper, G. J., and Aebi, U. (2000) Amyloid fibril formation from full-length and fragments of amylin. *J. Struct. Biol. 130*, 352–362.
20. Torrent, J., Alvarez-Martines, M. T., Harricane, M.-C., Heitz, F., Liautard, J.-P., Balny, C., and Lange, R. (2004) High pressure induces scrapie-like prion protein misfolding and amyloid fibril formation. *Biochemistry 43*, 7162–7170.
21. Tenidis, K., Waldner, M., Bernhagen, J., Fischle, W., Bergmann, M., Weber, M., Merkle, M. L., Voelter, W., Brunner, H., and Kaporniotu, A. (2000) Identification of a penta- and hexapeptide of islet amyloid polypeptide (IAPP) with amyloidogenic and cytotoxic properties. *J. Mol. Biol. 295*, 1055–1071.
22. Mazor, Y., Gilead, S., Benhar, I., and Gazit, W. (2002) Identification and characterization of a novel molecular-recognition and self-assembly domain within the islet amyloid polypeptide. *J. Mol. Biol. 322*, 1013–1024.
23. Azriel, R., and Gazit, E. (2001) Analysis of the minimal amyloid-forming fragment of the islet amyloid polypeptide. An experimental support for the key role of the phenylalanine residue in amyloid formation. *J. Biol. Chem. 276*, 34156–34161.
24. Lopes, D., Meister, A., Gohlke, A., Hauser, A., Blume, A., and Winter, R. (2007) Mechanism of islet amyloid polypeptide fibrillation at lipid interfaces studied by infrared reflection absorption spectroscopy. *Biophys. J. 93*, 3132–3141.
25. Engel, M., Yigittop, H., Elgersma, R., Risjkers, D., Liskamp, R., de Kruijff, B., Höppener, J., and Killian, J. (2006) Islet amyloid polypeptide inserts into phospholipid monolayers as monomer. *J. Mol. Biol. 356*, 783–789.
26. Nilsson, M., and Raleigh, D. (1999) Analysis of amylin cleavage products provides new insights into the amyloidogenic region of human amylin. *J. Mol. Biol. 294*, 1375–1385.
27. Cooper, G. J. (1994) Amylin compared with calcitonin gene-related peptide: Structure, biology, and relevance to metabolic disease. *Endocr. Rev. 15*, 163–2001.
28. Foguel, D., and Silva, J. L. (2004) New insights into the mechanisms of protein misfolding and aggregation in amyloidogenic diseases derived from pressure studies. *Biochemistry 43*, 11361–11370.
29. Silva, J. L., Cordeiro, Y., and Foguel, D. (2006) Protein folding and aggregation: Two sides of the same coin in the condensation of proteins revealed by pressure studies. *Biochim. Biophys. Acta 1764*, 443–451.
30. Zein, M., and Winter, R. (2000) Effect of temperature, pressure and lipid acyl-chain length on the structure and phase behaviour of phospholipid-gramicidin bilayers. *Phys. Chem. Chem. Phys. 2*, 4545–4551.
31. Desai, G., Panick, G., Zein, M., Winter, R., and Royer, C. A. (1999) Pressure-jump studies of the folding/unfolding of trp repressor. *J. Mol. Biol. 288*, 461–475.
32. Winter, R., Lopes, D., Grudzielanek, S., and Vogtt, K. (2007) Towards an understanding of the temperature/pressure configurational and free-energy landscape of biomolecules. *J. Non-Equilib. Thermodyn. 32*, 41–97.
33. Heremans, K., and Smeller, S. (1998) Protein structure and dynamics at high pressure. *Biochim. Biophys. Acta 1386*, 353–370.
34. Ulmer, H. M., Herberhold, H., Fahsel, S., Gänzle, M. G., Winter, R., and Vogel, R. F. (2002) Effects of pressure-induced membrane phase transitions on inactivation of HorA, an ATP-dependent multidrug resistance transporter, in *Lactobacillus plantarum*. *Appl. Environ. Microbiol. 68*, 1088–1095.
35. Cordeiro, Y., Kraineva, J., Ravindra, R., Lima, L. M., Gomes, M. P., Foguel, D., Winter, R., and Silva, J. L. (2004) Hydration and packing effects on prion folding and β-sheet conversion. High pressure spectroscopy and pressure perturbation calorimetry studies. *J. Biol. Chem. 279*, 32354–32359.
36. Jansen, R., Grudzielanek, S., Dzwolak, W., and Winter, R. (2004) High pressure promotes circularly shaped insulin amyloid. *J. Mol. Biol. 338*, 203–206.
37. Herberhold, H., Royer, C. A., and Winter, R. (2004) Effects of chaotropic and kosmotropic cosolvents on the pressure-induced unfolding and denaturation of proteins: An FT-IR study on staphylococcal nuclease. *Biochemistry 43*, 3336–3345.
38. Grudzielanek, S., Smirnovas, V., and Winter, R. (2006) Solvation-assisted pressure tuning of insulin fibrillation: From novel aggregation pathways to biotechnological applications. *J. Mol. Biol. 356*, 497–506.
39. Herberhold, H., Marchal, S., Lange, R., Scheyhing, C. H., Vogel, R. F., and Winter, R. (2003) Characterization of the pressure-induced intermediate and unfolded state of red-shifted green fluorescent protein: A static and kinetic FTIR, UV/VIS and fluorescence spectroscopy study. *J. Mol. Biol. 330*, 1153–1164.
40. Hummer, G., Garde, S., Garcia, A. E., Paulaitis, M. E., and Pratt, L. R. (1998) The pressure dependence of hydrophobic interactions is consistent with the observed pressure denaturation of proteins. *Proc. Natl. Acad. Sci. U.S.A. 95*, 1552–1555.
41. Jansen, R., Dzwolak, W., and Winter, R. (2005) Amyloidogenic self-assembly of insulin aggregates probed by high resolution atomic force microscopy. *Biophys. J. 88*, 1344–1353.
42. Lopes, D. H. J., Smirnovas, V., and Winter, R. (2008) Islet amyloid polypeptide and high hydrostatic pressure: towards an understanding of the fibrillization process. *Journal of Physics: Conference Series.* (in press).
43. Dzwolak, W., Ravindra, R., Lendermann, J., and Winter, R. (2003) Aggregation of bovine insulin probed by DSC/PPC calorimetry and FTIR spectroscopy. *Biochemistry 42*, 11347–11355.
44. Paladini, A. A., Jr., and Weber, G. (1981) Pressure-induced reversible dissociation of enolase. *Biochemistry 20*, 2587–2593.
45. Panick, G., Malessa, R., and Winter, R. (1999) Differences between the pressure- and temperature-induced denaturation and aggregation of β-lactoglobulin A, B, and AB monitored by FT-IR spectroscopy and small-angle X-ray scattering. *Biochemistry 38*, 6512–6519.
46. Dzwolak, W., Smirnovas, V., Jansen, R., and Winter, R. (2004) Insulin forms amyloid in a strain-dependent manner: An FT-IR spectroscopic study. *Protein Sci. 13*, 1927–1932.
47. Tatarek-Nossol, M., Yan, L. M., Schmauder, A., Tenidis, K., Westermark, G., and Kapurniotu, A. (2005) Inhibition of hIAPP amyloid-fibril formation and apoptotic cell death by a designed hIAPP amyloid-core-containing hexapeptide. *Chem. Biol. 12*, 797–809.
48. Jaikaran, E. T., Higham, C. E., Serpell, L. C., Zurdo, J., Gross, M., Clark, A., and Fraser, P. E. (2001) Identification of a novel human islet amyloid polypeptide β-sheet domain and factors influencing fibrillogenesis. *J. Mol. Biol. 308*, 515–525.
49. Gorovits, B. M., and Horowitz, P. M. (1998) High hydrostatic pressure can reverse aggregation of protein folding intermediates and facilitate acquisition of native structure. *Biochemistry 37*, 6132–6135.
50. St John, R. J., Carpenter, J. F., and Randolph, T. W. (1999) High pressure fosters protein refolding from aggregates at high concentrations. *Proc. Natl. Acad. Sci. U.S.A. 96*, 13029–13033.
51. Chatani, E., Kato, M., Kawai, T., Naiki, H., and Goto, Y. (2005) Main-chain dominated amyloid structures demonstrated by the effect of high pressure. *J. Mol. Biol. 352*, 941–951.
52. Dirix, C., Meersman, F., MacPhee, C. E., Dobson, C. M., and Heremans, K. (2005) High hydrostatic pressure dissociates early aggregates of $TTR_{105-115}$, but not the mature amyloid fibrils. *J. Mol. Biol.,* 903–909.
53. Ferrao-Gonzales, A. D., Souto, S. O., Silva, J. L., and Foguel, D. (2000) The preaggregated state of an amyloidogenic protein: Hydrostatic pressure converts native transthyretin into the amyloidogenic state. *Proc. Natl. Acad. Sci. U.S.A. 97*, 6445–6450.
54. Andersen, C. B., Otzen, D., Christiansen, G., and Rischel, C. (2007) Glucagon amyloid-like fibril morphology is selected via morphology-dependent growth inhibition. *Biochemistry 46*, 7314–7324.

BI800503J